The Deep Space Network Radio Astronomy User Guide

April 3, 2021

Document Owner: Joseph Lazio (Jet Propulsion Laboratory, California Institute of Technology)
©2021. California Institute of Technology. Government sponsorship acknowledged.

Contents

Changes to this Document . . . v
Acknowledgments . . . vi

1 Introduction **1**

2 Proposal Submission and DSN Scheduling **3**

3 70 m Subnetwork **4**
3.1 Antennas . . . 4
3.2 Efficiency and Gain . . . 4
3.3 Resolution . . . 5

4 34 m Subnetwork **7**
4.1 Antennas . . . 7
4.2 Efficiency and Gain . . . 8
4.3 Resolution . . . 9
4.4 Polarization . . . 10

5 Receiving Systems **12**
5.1 Radio Astronomical K Band (17 GHz–27 GHz) . . . 12
5.2 Radio Astronomical Q Band (38 GHz–50 GHz) . . . 13
5.3 L Band (1628 MHz–1708 MHz) . . . 13
5.4 S Band (2200 MHz–2300 MHz) . . . 13
5.5 X Band (8200 MHz–8600 MHz) . . . 14
5.6 Spacecraft Tracking K Band (25.5 GHz–27 GHz) . . . 14
5.7 Ka Band (31.8 GHz–32.3 GHz) . . . 14
5.8 Phase Calibration Tones for VLBI . . . 14

6 Signal Transport **20**

7 Backends **23**
7.1 Fast Fourier Transform Spectrometer (FFTS)-Madrid . . . 23
7.2 DSN Radio Astronomy Spectrometer-Canberra . . . 23
7.2.1 Level 0 Data . . . 24
7.2.2 Level 1 Data . . . 24
7.3 DSN Pulsar Processor-Canberra . . . 24
7.4 Open Loop Recorder . . . 25
7.5 VLBI Radio Astronomy (VRA) Assembly . . . 26

A Proposal Preparation and Observation Planning **27**

List of Figures

1.1 The DSN radio antennas and locations. 1

3.1 DSS-43, the 70 m antenna at the Canberra Complex 5

4.1 Illustration of key aspects of a DSN 34 m beam wave guide antenna 8

5.1 Overview of the DSS-43 radio astronomical K-band system. 16
5.2 Low-noise assembly ("front-end") for the DSS-43 K-band system 17
5.3 Downconverter for the DSS-43 K-band system 18
5.4 Q-band system installed at DSS-54. The feed horn that receives the radiation in the pedestal of the antenna is visible at the top of the picture, and the cyrogenic package housing the low-noise amplifiers in the top-center of the image, partially hidden behind the control board. (From Rizzo & García-Miró 2013.) 19

6.1 Signal transport at the Canberra Deep Space Communications Complex 21
6.2 Signal transport at the Madrid Deep Space Communications Complex 22

A.1 Visibility of sources from Canberra Deep Space Communications Complex 28
A.2 Visibility of sources from the Madrid Deep Space Communications Complex 29
A.3 Visibility of sources from the Goldstone Deep Space Communications Complex . . . 30

List of Tables

1.1 Deep Space Network Complexes 1

2.1 DSN Radio Astronomy proposal categories 3

3.1 70 m Aperture Efficiencies and Gains 6
3.2 70 m Antenna Beam Widths 6

4.1 Future DSN 34 m Beam Wave Guide Antennas 7
4.2 34 m Aperture Efficiencies and Gains 9
4.3 34 m Antenna Beam Widths 10
4.4 34 m Antenna Polarization Capabilities 11

7.1 DSN Radio Astronomy Spectrometer modes 24
7.2 Time Domain Radio Astronomy Instrumentation Recommendations 25
7.3 Time Domain Radio Astronomy Instrumentation Availability 25

Changes to this Document

Revision	Date	Summary
Original (v. 1)	2020 March	
Version 2	2020 November	proposal submission process updated; DSS-56 and DSS-65 descriptions added; updated status of DSS-43 L-band system; minor additions to DSS-54/Q-band system description; description of VLBI "phase cals" added; pulsar processor description updated, open loop recorder description added; minor corrections throughout

Acknowledgments

This document reflects the work and input of many individuals and builds upon a significant history of radio astronomy within NASA's Deep Space Network. Further, the radio astronomy activities within the Deep Space Network would not be possible without the efforts of the many engineers and technicians, at all three Complexes, who maintain the antennas and related infrastructure and have kept the Deep Space Network operating "around-the-clock" for over 50 years.

A likely incomplete list of those having provided notable efforts to DSN Radio Astronomy include

- Graham Baines (Canberra Deep Space Communications Complex)
- Alina Bedrossian (Jet Propulsion Laboratory, California Institute of Technology)
- Shinji Horiuchi (Canberra Deep Space Communications Complex)
- Thomas Kuiper (Jet Propulsion Laboratory, California Institute of Technology, *retired*)
- Danny Luong (Jet Propulsion Laboratory, California Institute of Technology)
- Luis Neira (Madrid Deep Space Communications Complex)
- Ricardo Rizzo (Centro de Astrobiología)
- Lawrence Teitelbaum (Jet Propulsion Laboratory, California Institute of Technology)
- Manuel Vazquez (Madrid Deep Space Communications Complex)
- Cristina Garcia-Miro
- Manuel Franco (*deceased*)
- Michael Klein (*deceased*)

We thank the authors of the Green Bank Telescope Proposal Guide and the Parkes Radio Telescope proposal guide for the guidance in producing this document. This work has made use of NASA's Astrophysics Data System.

This work was carried out at the Jet Propulsion Laboratory, California Institute of Technology, under a contract with the National Aeronautics and Space Administration (80NM0018D004).

Chapter 1

Introduction

The Deep Space Network (DSN) is the spacecraft tracking and communication infrastructure for NASA's deep space missions. It consists of three sites, approximately equally separated in (terrestrial) longitude, with multiple radio antennas at each site. Table 1.1 summarizes the key characteristics of the three sites; Figure 1.1 illustrates the locations of the various sites.

Table 1.1: Deep Space Network Complexes

Name	**Longitude**	**Latitude**	**Antennas**
Goldstone	$116^\circ\,46'\,44''$ W	$35^\circ\,16'\,53''$ N	DSS-14 (70 m), DSS-24, DSS-25, DSS-26 (34 m)
Canberra	$148^\circ\,58'\,56''$ E	$35^\circ\,24'\,06''$ S	DSS-43 (70 m), DSS-34, DSS-35, DSS-36 (34 m)
Madrid	$4^\circ\,14'\,59''$ W	$40^\circ\,25'\,45''$ N	DSS-63 (70 m), DSS-54, DSS-55 (34 m), DSS-65 (34 m)

Figure 1.1: The DSN radio antennas and locations.

The DSN antennas have a long history of radio astronomical observations. Contributions of DSN antennas to astronomical discoveries include the first identification of superluminal motion

(Cohen et al. 1971); demonstration of space-based very long baseline interferometry (VLBI) from which a clear indication of violation of the inverse Compton limit and constraints on the physical processes occurring in the central engines resulted (Levy et al. 1986, 1989; Linfield et al. 1989); the first detection of the infall and the inside-out collapse process during stellar formation (Velusamy, Kuiper, & Langer 1995; Kuiper et al. 1996); and demonstration of a continued gap in understanding of stellar structure and Galactic chemical evolution (the so-called "^{3}He problem") by detection of a hyperfine line of $^3He^+$ in the planetary nebula IC 418 (Guzman-Ramirez et al. 2016).

DSN antennas also have played an integral role in establishing and maintaining realizations of the International Celestial Reference Frame (ICRF, Fey et al. 2015; Charlot et al. 2020). The ICRF is not only the defining frame used for specifying the coordinates of all astronomical sources, it serves as the reference against which the plane-of-sky positions of deep space spacecraft are determined for navigation of NASA's deep space missions.

The focus of this document is on passive radio astronomical observations, of solar system objects other than the Sun or of celestial sources beyond the solar system, and including astrometric observations. Radar astronomy observations of solar system bodies is beyond the scope of this document but is described by Dvorsky et al. (1992), Slade et al. (2011), and Rodriguez-Alvarez et al. (2021) and references within. In a similar spirit, the transmit capabilities of the DSN antennas are not described here.

Much of this material is also presented in a series of documents contained in the DSN's Telecommunications Interfaces (2019), known colloquially as the 810-005 (with Modules 101, 104, and 211 of most relevance to radio astronomical observations), but it is presented here in a manner that is more common for radio astronomical observations.

Chapter 2

Proposal Submission and DSN Scheduling

This information is a brief overview of the proposal process. Full details are provided in a companion document, "DSN Radio Astronomy Proposal and Scheduling Guide."[1]

The DSN antennas can be used in a *stand alone* capacity or as part of a very long baseline interferometry (VLBI) observation. Three important principles apply to all proposals to use the DSN for radio astronomy:

- The prime responsibility of the DSN antennas is for spacecraft telemetry, tracking, and command (TT&C). While every effort will be made to accommodate projects that require time critical observations or observations at specific epochs, such observations can be challenging to schedule given the TT&C needs of the various missions that depend upon the DSN.
- The DSN schedules time four to six months in advance. While every effort will be made to accommodate proposals submitted less than six months in advance, review and scheduling of projects will be facilitated by submission six months in advance.
- It is a basic requirement for all proposals to use one or more DSN antennas for radio astronomy must specify how the proposed observations require some unique capability of the DSN.

There are three different categories of radio astronomical observations, which affect where proposals should be sent for evaluation and how approved projects appear on the DSN schedule (Table 2.1).

[1] https://deepspace.jpl.nasa.gov/about/commitments-office/science/

Table 2.1: DSN Radio Astronomy proposal categories

Category	**Summary**
Ground-Based Radio Astronomy (GBRA)	Proposals submitted to JPL, technical evaluation at JPL
European VLBI Network & Global VLBI (EGS)	Proposals for DSN antennas as part of a VLBI array, typically submitted to the EVN
Host County Radio Astronomy (HCRA)	Proposals submitted to respective host country (Australia and Spain) entities

Chapter 3

70 m Subnetwork

At each Complex is a 70 m diameter antenna, with a surface suitable for observations into the K band ($\approx$ 25 GHz).

3.1 Antennas

Each Complex hosts one 70 m diameter antenna. Constructed originally as 64 m diameter antennas based on the design for the Parkes Radio Telescope, the antennas were expanded to 70 m in diameter for the Voyager 2 Neptune encounter. The antenna optics are Cassegrain, with the radiation reflecting off the main reflector and a sub-reflector. The sub-reflector is rotated to direct the radiation into one of three "cones" where an appropriate receiver is located.

3.2 Efficiency and Gain

Table 3.1 presents the antenna gains, both referenced to an isotropic antenna (dBi) and in units of K Jy^{-1}. While the antenna surfaces are, in principle, capable of broad-band operation at least to the K band, in practice, the DSN frequency coverage for the 70 m antennas is dictated by a combination of deep space telecommunications needs and historical radio astronomical interests, both at Caltech Campus and JPL and within the larger very long baseline interferometry (VLBI) community. Specifically, the S- and X bands are standard deep space telecommunications bands; the L band has been used for previous deep space missions (primarily to Venus), but is not used currently for any deep space missions; and the K band covers, but is broader than, a spectral allocation used for missions beyond geosynchronous orbit (GEO), but not to the 2 million km "threshold" identified by the International Telecommunications Union (ITU).

The antenna gains do change with elevation, in a frequency-dependent manner.

S band The estimated losses due to elevation changes do not exceed 0.3 dB (7%), with the peak gain occurring at elevations near 40°.

X band The estimated losses due to elevation changes do not exceed 0.8 dB (20%), with the peak gain occurring at elevations of about 40°.

K band The peak gain occurs at elevations of about 40°.

Observations at other frequencies are, in principle, possible. For instance, a ultra-high frequency (UHF) band system, operating near 0.4 GHz, was once mounted for a combination of spacecraft

Figure 3.1: DSS-43, the 70 m antenna at the Canberra Complex. Two of the three receiver cones are visible below the subreflector; the third is hidden behind the two visible cones. (In the background is a 34 m beam wave guide antenna.)

telecommunications and potential radio astronomical observations. Installation of systems at other frequencies can be considered; discussions with contacts identified earlier in this document (§2) are encouraged.

3.3 Resolution

The beamwidths of the antennas are well modeled by a symmetric function of $\theta = 16.2'(1\,\mathrm{GHz}/\nu)$ or $\theta = 0.54'(\lambda/1\,\mathrm{cm})$. Table 3.2 summarizes the half-power beamwidth of the antennas for the specific operational frequencies.

Table 3.1: 70 m Aperture Efficiencies and Gains

Band	**Center Frequency (GHz)**	**Frequency Range (GHz)**	**Antenna**	**Gain (dBi)**	**Gain (K Jy^{-1})**
L[a,b]	1.668	1.628–1.708	all	61.04 ± 0.3	1.18
S	2.295	2.2–2.3	all	63.59 ± 0.1	1.12
			DSS-14 (Goldstone)	74.55 ± 0.1	1.04
X[c]	8.42	8.2–8.6	DSS-43 (Canberra)	74.63 ± 0.1	1.06
			DSS-63 (Madrid)	74.66 ± 0.1	1.07
K	22	18–27	DSS-43[d] (Canberra)	80.2	0.56
			DSS-63[e] (Madrid)	78.2	0.36

[a] Left circular polarization (LCP) only; right circular polarization (RCP) is possible, with prior arrangement to change the mechanical configuration of the feed.

[b] The L-band feed on DSS-43 (Canberra) was removed as part of the replacement of the X-band Cone. Re-installation of the feed is scheduled for early 2022.

[c] With S-X dichroic extended to enable simultaneous, dual-band observations, there is a loss at X band of between 0.2 dB and 0.5 dB, equivalent to a loss of no more than about 10%.

[d] Based on measurements in 2021 February

[e] From Rizzo et al. (2012)

NOTE—This table is adapted from Tables 2 and 4 of 810-005, Module 101G.

Table 3.2: 70 m Antenna Beam Widths

Band	**Center Frequency (GHz)**	**Antenna**	**Beam Width (arc minutes)**
L band	1.668	all	9.72 ± 0.96
S band	2.295	all	7.08 ± 0.72
X band	8.42	all	1.92 ± 0.18
K band	22	DSS-43 DSS-63	0.74

This table is adapted from Table 2 of 810-005, Module 101G.

Chapter 4

34 m Subnetwork

Each Complex hosts multiple 34 m diameter antennas (Table 1.1), with surfaces suitable for observations as high as 45 GHz. In addition to the antennas described below, the DSN operates DSS-13 as a "research & development" antenna. This antenna was originally a prototype for the 34 m beam wave guide design and broadly has the capabilities described in the remainder of this chapter. This antenna is currently intended for initial testing of a concept for integrating radio frequency and laser (optical) communications by outfitting a portion of its surface with surfaces that are reflective for the near-infrared lasers intended for laser communications. While it may be available for radio astronomical observations, it is recommended that individuals interested in potential observations contact the authors of this document to confirm availability and performance.

4.1 Antennas

Most of the DSN's 34 m antennas are *beam wave guide* (BWG) antennas, in which the radiation is directed by a sub-reflector into a beam wave guide and into a subterranean pedestal room. This design allows for multiple receivers to be operated and maintained without needing access to the antenna structure itself as well as being able to locate the sensitive receivers in a more stable location (pedestal) rather than on a moving antenna.

The DSN is in the process of increasing the number of 34 m BWG antennas, via the DSN Aperture Enhancement Project (DAEP). Table 4.1 summarizes the planned construction and capabilities of future 34 m antennas.

Table 4.1: Future DSN 34 m Beam Wave Guide Antennas

Antenna	**Complex**	**Planned Date**	**Bands**
DSS-53	Madrid	2021 January[a]	X, Ka
DSS-23	Goldstone	2024 September	X, Ka
DSS-33	Canberra	2026 September	X, Ka

[a] Delivery of this antenna has been slowed by the COVID-19 global pandemic.

This table is adapted from Section 3 of 810-005, Module 104L.

In addition to the beam wave guide antennas, the DSN continues to operate one "high efficiency antenna," DSS-65. Its description is derived from the fact that, at the time of its construction, there were lower efficiency antennas in operation. Today the gain of DSS-65 is similar to that of

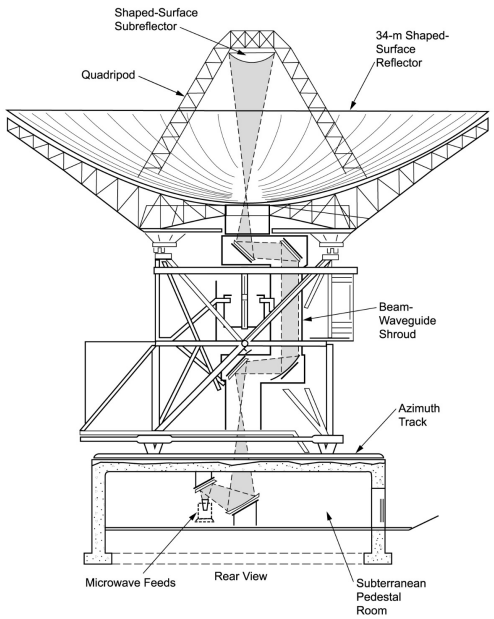

Figure 4.1: (*left*) Illustration of key aspects of a DSN 34 m beam wave guide antenna. (From Imbriale 2003.) (*right*) DSS-36, the most recently constructed 34 m beam wave guide antenna in Australia. The beam wave guide shroud is apparent behind the reflector.

the 34 m BWG antennas, but its description as a "high efficiency (HEF) antenna" persists.

4.2 Efficiency and Gain

Table 4.2 presents the antenna gains, both referenced to an isotropic antenna (dBi) and in units of K Jy^{-1}. At present, the DSN frequency coverage for the 34 m antennas is dictated solely by spacecraft telecommunications needs, with the exception of DSS-54 at MDSCC, at which there is a radio astronomical Q band system installed (§5.2). Specifically, the S-, X-, and Ka bands are standard deep space telecommunications bands; there is also a K band capability for "near Earth" telecommunications.[1] Further, the frequency coverage is not uniform at all antennas, with some antennas having frequency capabilities that others do not.

These values do change with elevation, in a frequency-dependent manner.

S band The estimated losses due to elevation changes do not exceed 0.4 dB (10%), with the peak gain occurring at elevations near 40°.

X band The estimated losses due to elevation changes do not exceed 0.6 dB (15%), with the peak gain occurring at elevations of about 50°.

K band The estimated losses due to elevation changes do not exceed 1.2 dB (30%) under good weather conditions but can approach 4 dB (over a factor of 2) under poor weather conditions. The peak gain occurs at elevations of about 50°.

[1]The boundary between deep space and near-Earth is defined by the International Telecommunications Union as 2 million km.

Table 4.2: 34 m Aperture Efficiencies and Gains

Band	**Frequency Range (GHz)**	**Antenna**	**Gain (dBi)**	**Gain (K Jy^{-1})**
S	2.2–2.3	DSS-24, DSS-26	$56.74^{+0.1}_{-0.2}$	0.24
		DSS-34, DSS-36	$56.74^{+0.1}_{-0.2}$	0.24
		DSS-54, DSS-56	$56.73^{+0.1}_{-0.2}$	0.23
		DSS-65	56.07 ± 0.25	0.20
X[a]	8.4–8.5	DSS-24	$68.24^{+0.1}_{-0.2}$	0.24
	8.2–8.6	DSS-25, DSS-26	$68.3^{+0.1}_{-0.2}$	0.25
	8.2–8.6	DSS-34, DSS-35, DSS-36	$68.3^{+0.1}_{-0.2}$	0.25
	8.2–8.6	DSS-54, DSS-55, DSS-56	$68.3^{+0.1}_{-0.2}$	0.25
	8.2–8.6	DSS-65	68.41 ± 0.2	0.25
K	25.5–27	DSS-24, DSS-26	$77.2^{+0}_{-0.2}$	0.2
		DSS-34, DSS-36	$77.2^{+0}_{-0.2}$	0.2
		DSS-54, DSS-56	$77.2^{+0}_{-0.2}$	0.2
Ka	31.8–32.3	DSS-25, DSS-26	$79.0^{+0.3}_{-0.3}$	0.2
		DSS-34, DSS-35, DSS-36	$79.0^{+0.3}_{-0.3}$	0.2
		DSS-54, DSS-55, DSS-56	$79.0^{+0.3}_{-0.3}$	0.2
Q	38–50	DSS-54	80.5	0.15

[a]With S-X dichroic extended to enable simultaneous, dual-band observations, there is a loss at X band of 0.05 dB, equivalent to a loss of no more than about 1%.
NOTE—This table is adapted from Tables 1, 5, 6, and 7 in 810-005, Module 104L and Table 3 in 810-005, Module 103C.

Ka band The estimated losses due to elevation changes do not exceed 2 dB (58%) under good weather conditions but can approach 4 dB (over a factor of 2) under poor weather conditions. The peak gain occurs at elevations of about 50°.

Further, at K-, Ka-, and Q bands, the antenna gains can be affected significantly by the zenith opacity due to the amount of water vapor in the atmosphere above the antenna. Under generally clear conditions, the additional zenith opacity does not exceed 5% at either band. However, under cloudy conditions zenith opacities can be 10%. In general, opacities tend to be lowest at Goldstone, due to its arid climate, and highest at Canberra, with Madrid showing intermediate values.

4.3 Resolution

Table 4.3 summarizes the half-power beamwidth of the antennas for the specific operational frequencies.

Table 4.3: 34 m Antenna Beam Widths

Band	**Antenna**	**Beam Width**
	DSS-24, DSS-26	
S	DSS-34, DSS-36	14.5′
	DSS-54, DSS-56, DSS-65	
X	all	4′
	DSS-24	
K	DSS-34, DSS-36	1.3′
	DSS-54, DSS-56	
	DSS-25, DSS-26	
Ka	DSS-34, DSS-35, DSS-36	1′
	DSS-54, DSS-55, DSS-56	
Q	DSS-54	43″

NOTE—This table is adapted from Tables 5, 6, and 7 in 810-005, Module 104L and Table 3 in 810-005, Module 103C.

4.4 Polarization

In general, only a single polarization is available, which can be either right circular polarization (RCP) or left (LCP). Table 4.4 summarizes the antennas for which there are *exceptions*.

Table 4.4: 34 m Antenna Polarization Capabilities

Antenna	**Band**	**Polarization**
DSS-24 (Goldstone)	X	RCP and LCP
DSS-25 (Goldstone)	X	RCP and LCP[a]
DSS-26 (Goldstone)	X	RCP and LCP
DSS-34 (Canberra)	X	RCP and LCP
DSS-35 (Canberra)	X	RCP and LCP
DSS-35 (Canberra)	X	RCP and LCP
DSS-55 (Madrid)	X	RCP and LCP
DSS-56 (Madrid)	X	RCP and LCP
DSS-25 (Goldstone)	Ka	RCP and LCP
DSS-26 (Goldstone)	Ka	RCP and LCP
DSS-34 (Canberra)	Ka	RCP and LCP
DSS-35 (Canberra)	Ka	RCP and LCP
DSS-36 (Canberra)	Ka	RCP and LCP
DSS-54 (Madrid)	Ka	RCP and LCP
DSS-55 (Madrid)	Ka	RCP and LCP
DSS-56 (Madrid)	Ka	RCP and LCP
DSS-54 (Madrid)	Q	RCP and LCP

[a]One, selectable polarization will have less sensitivity than the other

NOTE—If not listed, an antenna should be assumed to have only either RCP or LCP.

This table is adapted from Table 1 in 810-005, Module 104L and Table 3 in 810-005, Module 103C.

Chapter 5

Receiving Systems

Echoing the discussion in §3.2, the current suite of receivers reflects both the DSN's mission for spacecraft tracking and historical precedent. The order of this section is in terms of those receivers and bands developed primarily for radio astronomy observations followed by those that are standard for spacecraft TT&C but also available for radio astronomical observations.

5.1 Radio Astronomical K Band (17 GHz–27 GHz)

Both DSS-43 (Canberra) and DSS-63 (Madrid) are equipped with K-band systems. The focus of this section is on the DSS-43 system, as it is the more capable. The DSS-63 system is suitable for VLBI observations, but does not have as wide of a band nor the suite of backends available at DSS-43 (Chapter 7).

DSS-43 is equipped with a radio astronomical system operating in the 17 GHz–27 GHz band. Figure 5.1 provides an overview of the system, and Figures 5.1–5.3 show the major components of the system. Kuiper et al. (2019) provide a more detailed description of this system.

The *LNA Assembly* (or "front-end") contains two feed horns, allowing for simultaneous observations of both a target source and a secondary position (e.g., for calibration purposes). Each feed horn produces linear polarization, and the two feed horns are separated by $2.1'$ (equivalent to 2.8 half-power beamwidths at 22 GHz). Each linear polarization from each feed horn is connected to a cryogenic LNA. Ambient temperature microwave absorbers and phase calibration signals (with 1 MHz or 4 MHz frequency combs) can be inserted into the signal path for calibration purposes.

The *Downconverter* receives the output from the LNA Assembly and produces intermediate frequencies (IFs). There are four signal chains (labelled E1, H1, E2, and H2 for the E- and H-plane polarizations of Feeds 1 and 2), and switches allow the signals to be switched in a manner to cancel gain profiles. Each signal chain is then passed to a set of bandpass filters, producing 2 GHz sub-bands centered at 18 GHz, 20 GHz, 22 GHz, 24 GHz, and 26 GHz. Following the bandpass filters, polarization converters allow the signals to be converted from linear polarization to circular polarization, if desired. Finally, local oscillators (LOs) are mixed with the sub-bands to produce 1 GHz IFs. These 1 GHz IFs are then transported by fiber optic cables from the antenna to the Signal Processing Center for detection and post-processing.

Estimates of the receiver temperature, extrapolated to outside the atmosphere, are $T_{\rm RX} = 29$ K, with approximately 10% uncertainty or variation from feed-polarization channel to channel. Under near-ideal conditions (clear skies and cold ambient temperatures), total system temperatures $T_{\rm sys}$ approaching 40 K have been measured.

5.2 Radio Astronomical Q Band (38 GHz–50 GHz)

The DSS-54 (34 m) antenna at the Madrid DSCC is equipped with a Q band receiving system, developed under the auspices of the Spanish host country radio astronomy community (Figure 5.2). This material is extracted from a larger discussion by Rizzo et al. (2012).

The Q-band front-end has a notional frequency range of 38 GHz–50 GHz per polarization, though the slightly restricted frequency range of 39 GHz–49 GHz provides better sensitivity. At the front-end, the band is mixed with an LO at 62 GHz, providing 12 GHz of transported bandwidth from 12 GHz to 24 GHz. At the IF processor, this transported bandwidth is split into two 8 GHz wide sub-bands (labeled LO and HI, respectively). The LO sub-band is 12 GHz–20 GHz, and the HI sub-band is 18 GHz–26 GHz. The IF processor further downconverts each sub-band to a tunable 1.5 GHz baseband per polarization.

The final output of the Q-band system is thus four simultaneous signals, 1.5 GHz baseband right- and left-circular polarization in the HI sub-band (mapping to sky frequencies 44 GHz–38 GHz) and 1.5 GHz baseband right- and left-circular polarization in the LO sub-band (mapping to sky frequencies 42 GHz–50 GHz). Because of the processing within the IF processor, the HI sub-band signals are mirrored in frequency.

5.3 L Band (1628 MHz–1708 MHz)

The 70 m antennas are equipped with an L-band feed, normally configured to receive left circular polarization (LCP) though, with sufficient advance notice, it can be reconfigured (manually) to receive RCP. The position of the L-band feed requires that the antenna subreflector be rotated to illuminate the L-band feed, which prevents other frequencies from being simultaneously available.

For DSS-14 and DSS-63, the L-band feed is a so-called "Potter horn" (Potter 1963), which is a relatively narrowband design optimized for 1.668 GHz and a single polarization. Experience suggests that somewhat wider bandwidths than the original design may be able to be obtained. For DSS-43, a "wide-band" feed was designed (Hoppe et al. 2015) and installed. This feed was removed as part of the 2020 Depot Level Maintenance. Current plans are that it will be reinstalled in early 2022, other components of the L-band system (e.g., LNAs, signal transport) may not be installed at that time.

The low-noise amplifiers (LNAs) are cooled HEMT devices, with typical noise temperatures of 27 K.

After amplification, the L-band signal is up-converted to S band and sent to the S-band Signal Distribution Assembly for subsequent downconversion and transmission through the S-band transmission system.

5.4 S Band (2200 MHz–2300 MHz)

All 70 m antennas and at least one 34 m antenna at each Complex are equipped with S-band receiving systems. These systems are designed primarily for spacecraft TT&C, hence their relatively narrow bandwidths relative to current radio astronomical systems.

The main reflector illuminates the S-band feed via an S-X dichroic plate. Following the feed is an orthomode junction, enabling dual polarization observations. However, because of the TT&C needs, one of the polarizations is always fed to a diplexer resulting in a slightly higher system temperature for that polarization ($\approx$ 10% higher). The signals are then amplified by an LNA, cooled HEMT

devices, and fed to the S-band signal distribution assembly before being downconverted to an intermediate frequency (IF) for signal transport (Chap. 6).

Typical (zenith) system temperatures are 17 K (DSS-14 and DSS-43) and 20 K (DSS-63) and approximately 22 K (34 m beam waveguide antennas) and at least 34 K (DSS-65). Because of the S-X dichroic plate, there is also a configuration enabling dual frequency-single polarization observations between S- and X bands. The dual S-X capability increases the noise S-band temperature by approximately 5 K.

Experience suggests that the S-band systems can be affected significantly by radio frequency interference (RFI).

5.5 X Band (8200 MHz–8600 MHz)

All 70 m antennas and at least one 34 m antenna at each Complex are equipped with X-band receiving systems. These systems are designed primarily for spacecraft TT&C, hence their relatively narrow bandwidths relative to current radio astronomical systems. In particular, the X-band coverage at DSS-24 is even more restricted than the general 34 m antennas, being restricted to the range 8400 MHz–8500 MHz.

The X-band feed is followed by a diplexing junction in order to allow for injection of transmissions (for spacecraft TT&C), by an orthomode junction in order to enable dual polarization observations, and by LNAs that are cooled HEMT devices.

Typical (zenith) system temperatures are 17 K (70 m antennas). With the S-X dichroic plate extended, dual frequency-single polarization observations between S- and X bands. The dual S-X capability increases the X-band noise temperature by approximately 1 K.

5.6 Spacecraft Tracking K Band (25.5 GHz–27 GHz)

Within the DSN, this band is also called the "near-Earth Ka band" or the "Ka2 band."

At least one 34 m (BWG) antenna at each Complex is equipped with a K-band receiving system. These systems are designed primarily for spacecraft TT&C, hence their relatively narrow bandwidths relative to current radio astronomical systems.

This receiving system can be used in combination with the TT&C S-band receiving system (§5.4).

5.7 Ka Band (31.8 GHz–32.3 GHz)

Most of the 34 m (BWG) antenna at each Complex are equipped with a Ka-band receiving system. These systems are designed primarily for spacecraft TT&C, hence their relatively narrow bandwidths relative to current radio astronomical systems.

This receiving system can be used in combination with the TT&C X-band receiving system (§5.4. The simultaneous reception of X- and Ka-band signals involves the extension of a dichroic plate, which produces a small decrease in the antenna gain (≈ 0.15 dBi).

5.8 Phase Calibration Tones for VLBI

For all of the 70 m antennas, and for DSS-65, it is possible to inject a phase calibration tone ("phase cals") into the signal path before the LNA. Most of the 34 m beam wave guide antennas

are equipped with "phase cals" for X- and Ka-band signal paths (with the possible exceptions of DSS-24 and DSS-36). "Phase cals" for S- and X-band are available at DSS-26, DSS-34, and DSS-54.

The S- and X-band "phase cals" are spaced by 1 MHz. The X- and Ka-band "phase cals" are selectable, either at 1 MHz or 4 MHz, with a 4 MHz spacing being the default selection.

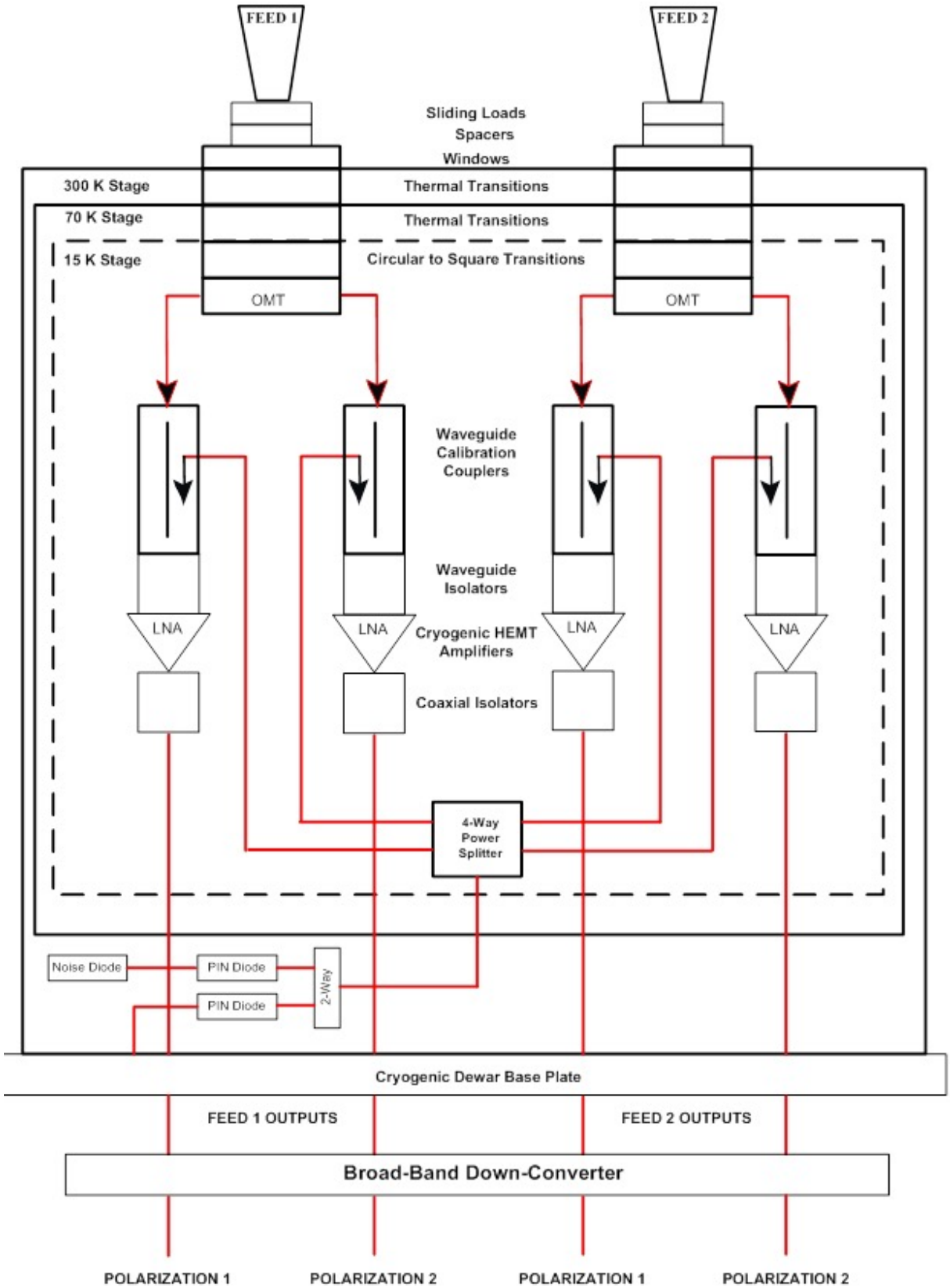

Figure 5.1: Overview of the DSS-43 radio astronomical K-band system.

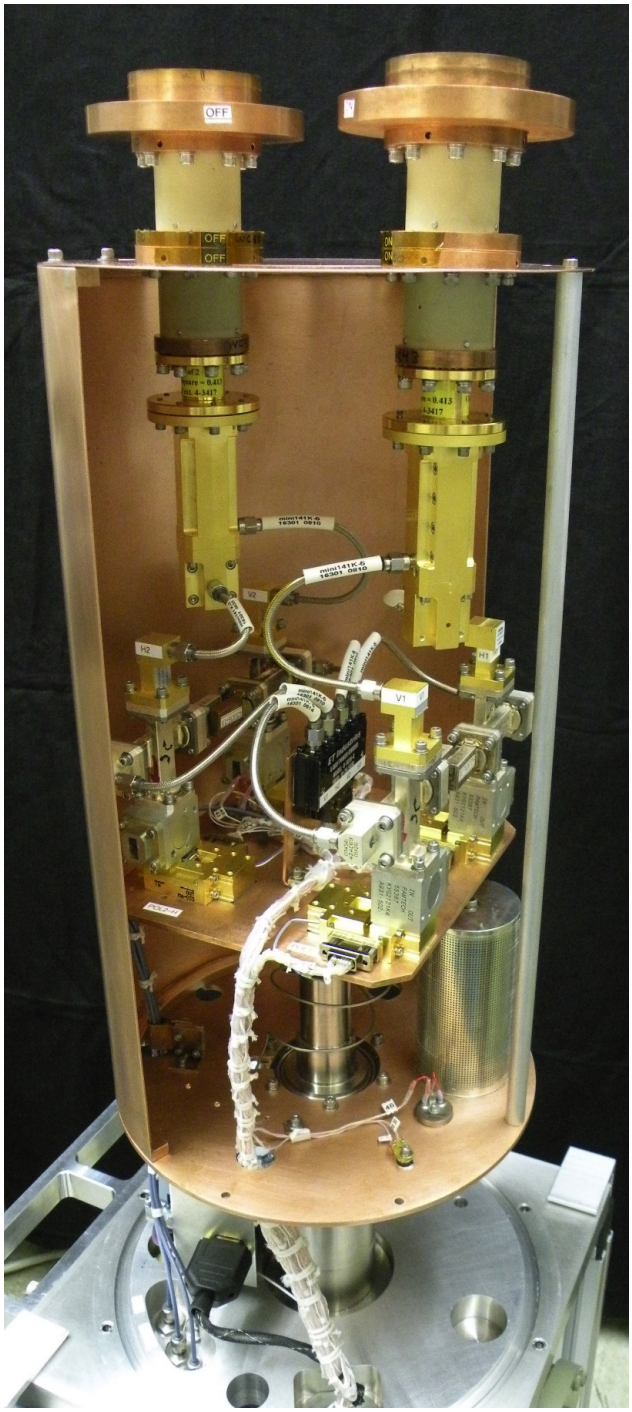

Figure 5.2: Low-noise assembly ("front-end") for the DSS-43 K-band system. Visible are the two feeds at top, the waveguide calibration couplers (vertical rectangular units), and the plane on which the LNAs and 4-way power splitter are mounted.

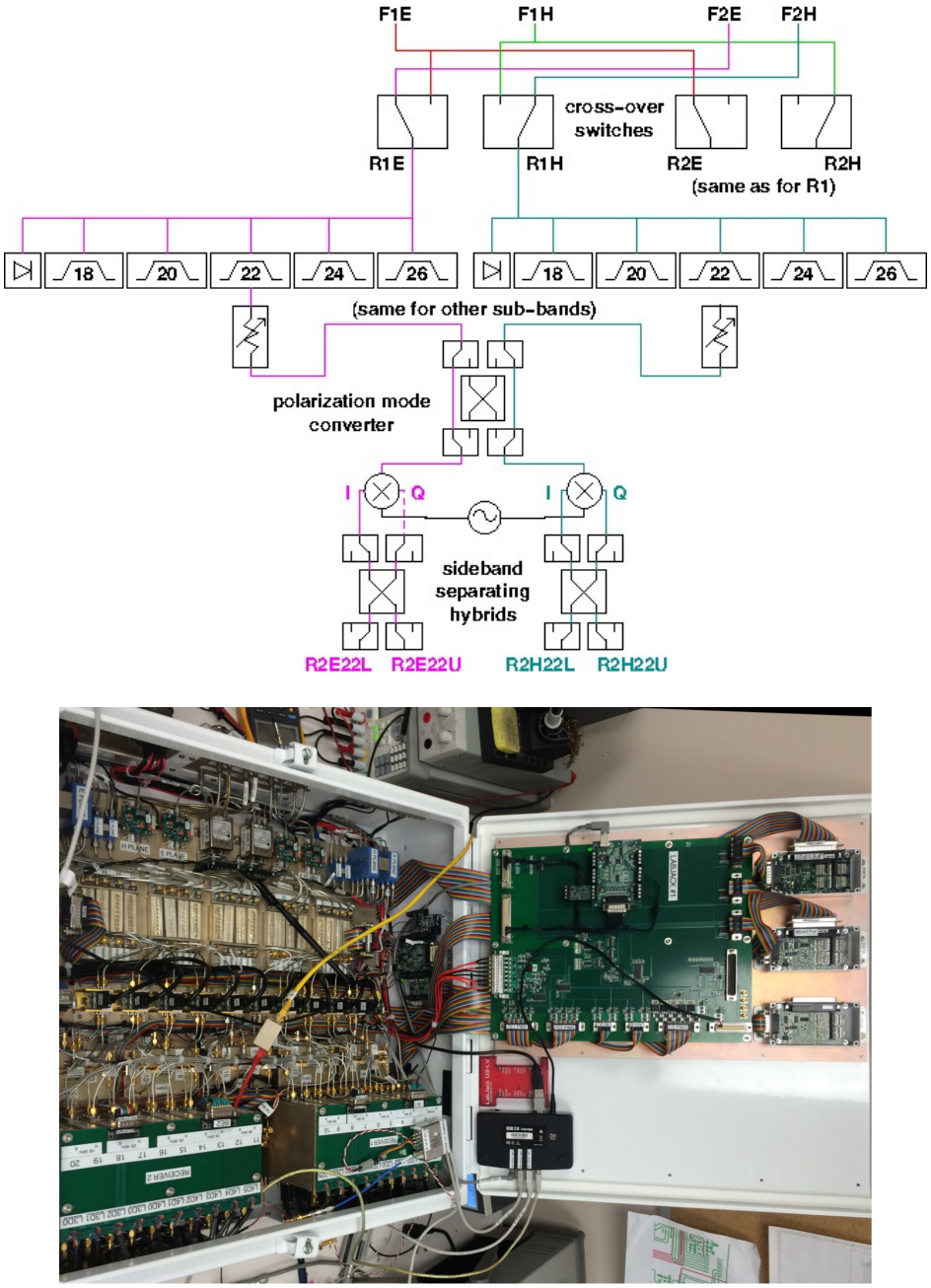

Figure 5.3: Downconverter for the DSS-43 K-band system.(*top*) Block diagram;(*bottom*) Rotated view of the unit prior to mounting on the antenna. Matching the orientation of the above schematic, the four inputs from the outputs of the feed horns are on the top of this image, with signals traveling "downward." The downconverter modules, producing the 40 IF outputs, are the green boxes at the bottom.

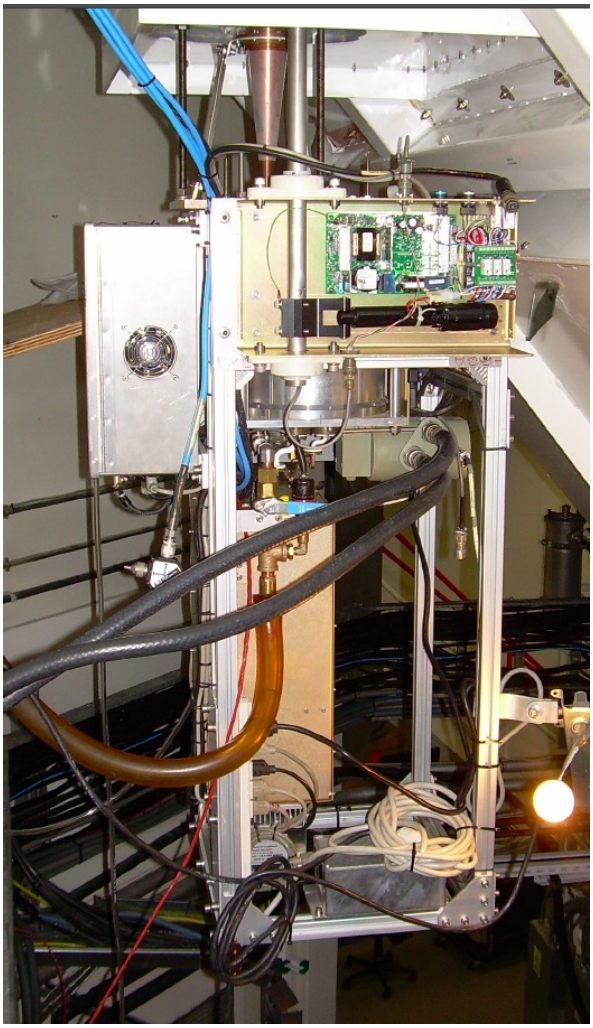

Figure 5.4: Q-band system installed at DSS-54. The feed horn that receives the radiation in the pedestal of the antenna is visible at the top of the picture, and the cyrogenic package housing the low-noise amplifiers in the top-center of the image, partially hidden behind the control board. (From Rizzo & García-Miró 2013.)

Chapter 6

Signal Transport

Following conditioning at the antenna, the signals are downconverted from the sky frequency to an intermediate frequency (IF). The (analog) IF signals are transported over fiber optic links from the antenna to the Signal Processing Center (SPC). Typically, the IF is 500 MHz wide, from 100 MHz to 600 MHz, though it can be narrower at S band. (The S-band allocation for deep space telecommunications is only 10 MHz wide.)

Radio astronomical systems can employ slightly different signal transport systems than the standard DSN systems, but the overall signal flow is substantially similar.

Figures 6.1–6.2 provide a graphical view of the signal transport from the antennas to the various processing backends for each Complex. For clarity, two figures are shown for each complex, one for the 70 m antenna at that Complex and one for the 34 m beam waveguide antennas.

For the DSS-43 K-band system, following downconversion, the signals are transported in 1 GHz bands over fiber optic links to the Canberra Signal Processing Center.

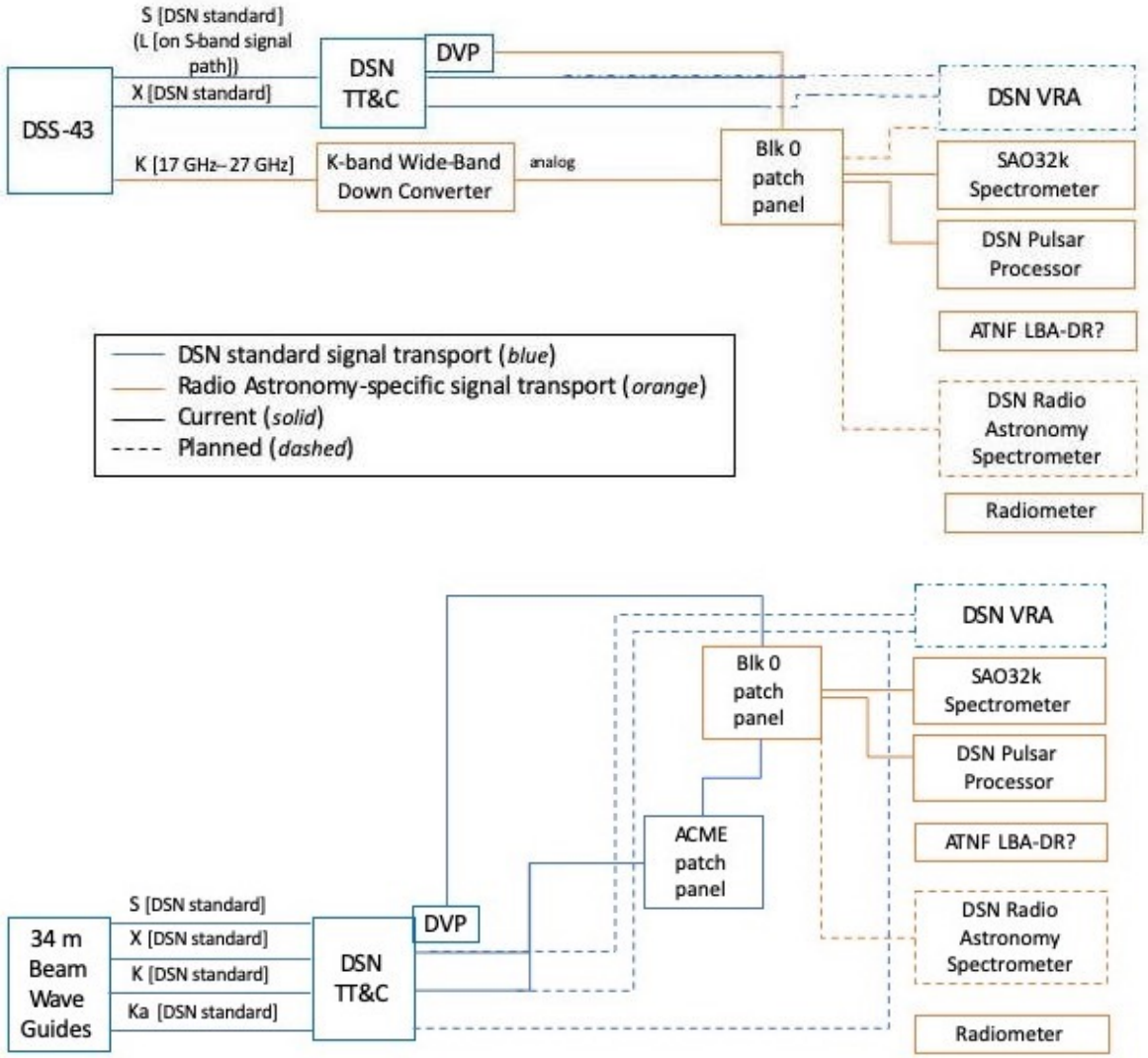

Figure 6.1: *top* Signal transport for DSS-43 at the CDSCC.*bottom* Signal transport for 34 m beam waveguide antennas at the CDSCC. Not every 34 m beam waveguide antenna offers all frequencies, viz. Table 4.2.

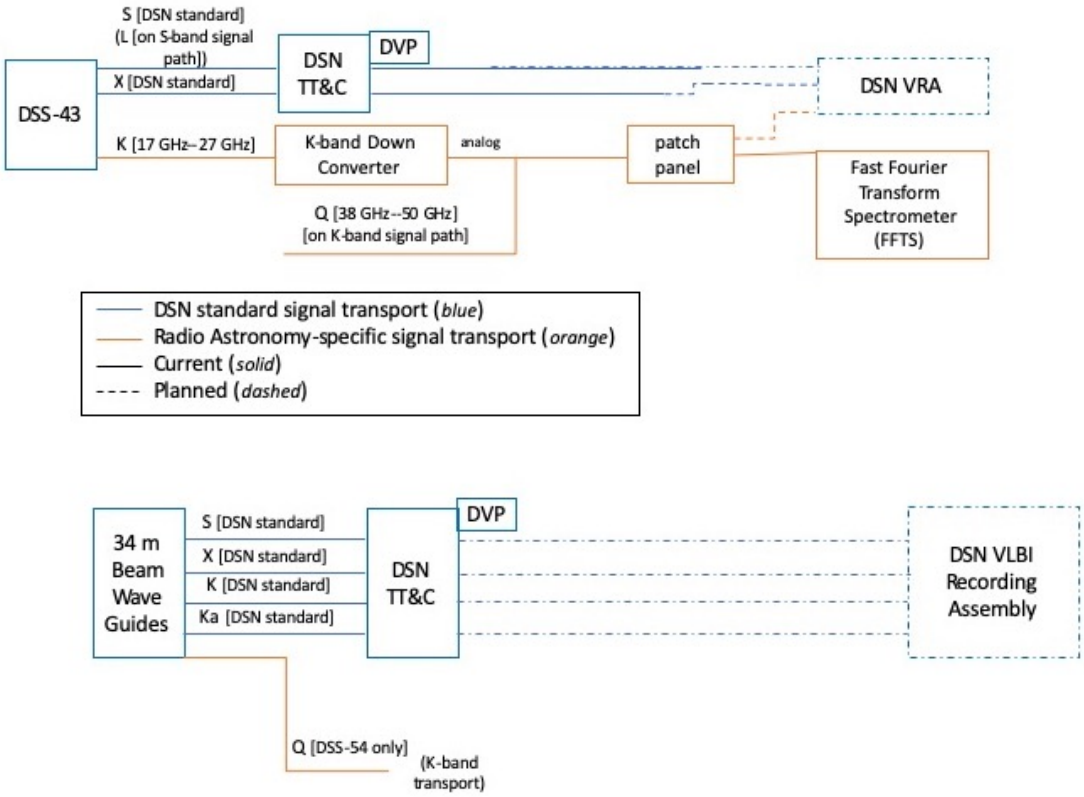

Figure 6.2: *top* Signal transport for DSS-63 at the MDSCC.*bottom* Signal transport for 34 m beam waveguide antennas at the MDSCC. Not every 34 m beam waveguide antenna offers all frequencies, viz. Table 4.2.

Chapter 7

Backends

The various DSN Complexes host different processing backends, dictated largely by previous scientific interests of Caltech and JPL staff and external users. Each backend is summarized briefly; in many cases, there are more detailed publications providing additional information.

For the backends at Canberra, they are typically configured to work with the radio astronomical K-band system, though, in principle, they can accept input from any of the available bands (radio astronomical or spacecraft TT&C) at the Complex (Chapter 5).

The development of additional backends or user-provided backends is both feasible and encouraged. Interested individuals should contact DSN Radio Astronomy staff for discussions and assessment of feasibility.

7.1 Fast Fourier Transform Spectrometer (FFTS)-Madrid

The Fast Fourier Transform Spectrometer (FFTS) is a Spanish host-country backend, installed at the Madrid Complex. This material is extracted from a longer description by Rizzo et al. (2012).

The FFTS accepts four analog 1.5 GHz baseband inputs, corresponding to the right- and left-circularly polarized HI and LO sub-bands for the Madrid Complex (§5.2). Each baseband is digitized, with an 8-bit digitizer, and then transformed to the frequency domain via a four-tap polyphase filterbank. The default configuration is 8192 frequency channels, providing 183 kHz spectral resolution across the full 1.5 GHz bandwidth, equivalent to a velocity resolution of 1.24 km s^{-1} at a fiducial frequency of 44 GHz. Higher spectral resolutions across a narrower bandwidth may also be available upon request.

7.2 DSN Radio Astronomy Spectrometer-Canberra

The DSN Radio Astronomy Spectrometer is installed at the Canberra Complex. This material is extracted from Virkler et al. (2020).

The DSN Radio Astronomy Spectrometer is designed specifically to accommodate the output of the Radio Astronomical K-band system, but, in principle, can process any of the outputs from any of the systems at the Canberra Complex. Table 7.1 summarizes the available modes for this spectrometer.

Data from the Radio Astronomy Spectrometer will be provided in single-dish FITS (SDFITS) format (Garwood 2000) in a series of levels reflecting increasing data processing.

Table 7.1: DSN Radio Astronomy Spectrometer modes

Mode	Summary
1	32k spectral points, FFT-based
2	8k spectral points, polyphase filter-based
3	512k spectral points [TBC]

7.2.1 Level 0 Data

The header contains relevant data about the antenna and details of the observations.

The primary data consist of the spectra acquired during the observation, with each entry being the spectrum for each scan.

Additional data tables (structured as FITS `BINTABLE`) are provided, which contain information about the observation that is used for subsequent processing to higher level data products. One data table provides the antenna's elevation as a function of time during each scan, and a second data table provides an estimate of the system temperature $T_{\rm sys}$ as a function of time during each scan.

7.2.2 Level 1 Data

These data products are intended to be a notional processing of the Level 0 data, in a manner that is consistent with producing data products sufficient for analysis and publication but also for alternate or additional processing. The intent is to provide a basic estimate of the antenna temperature using the standard position-switching technique,

$$T^*_{\rm ant} = \frac{T_{\rm on} - T_{\rm off}}{T_{\rm off}} T_{\rm sys}, \tag{7.1}$$

where $T_{\rm on}$ is the measured temperature (power) toward a source, $T_{\rm off}$ is the measured temperature (power) toward an "off" position, and $T_{\rm sys}$ is the system temperature.

Level 1a Data

The Level 1a data product performs the first portion of the calibration, forming the factor $T_{\rm on} - T_{\rm off}/T_{\rm off}$ using the *nearest-neighbor* "off" scan. This division in the calibration is structured in this manner for a number of motivations. With this initial "ON−OFF" calculation an investigator can assess the calibration at this stage, there may be some cases in which only relative calibration (without the system temperature) may be valuable, and there are alternate approaches to identifying the "off" scan (e.g., linear interpolation between the two "off" scans nearest in time).

Level 1b Data

The Level 1b data product uses the Level 1a data product and an estimate of the system temperature $T_{\rm sys}$ to form the antenna temperature $T^*_{\rm ant}$ of equation (7.1).

7.3 DSN Pulsar Processor-Canberra

The DSN Pulsar Processor is installed at the Canberra Complex. This material is extracted from a longer description by Kocz et al. (2016).

Table 7.2: Time Domain Radio Astronomy Instrumentation Recommendations

Observation	**Recommended Backend**
Low, Modest DM Searches	Pulsar Backend
High DM Searches	Pulsar Backend
Single-Pulse Studies, recycled and millisecond pulsars	Open Loop Recorder
Single-Pulse Studies, slow pulsars, FRBs	Pulsar Backend

Table 7.3: Time Domain Radio Astronomy Instrumentation Availability

Backend	**Antenna Availability**
Pulsar Backend	70 m or 34 m
Open Loop Recorder	34 m only

The Pulsar Backend is designed for high-speed, near-real time searching of pulsar and fast radio burst signals, and it is built on ROACH2 hardware platforms. The system was designed to exploit the K-band system, and it can accommodate up to 16 subbands, each up to 1 GHz wide. Standard use would be to acquire 8 GHz of bandwidth in two polarizations, for which the current configuration of the system provides 16 384 spectral channels with time resolution as fine as 32 μs with a 16-bit per sample dynamic range.

The system makes use of a 10 MHz reference and a pulse per second (PPS) signal to keep all components synchronized. The ADC boards do not have a large built-in gain control. In order to provide for gain control, a set of variable attenuators are used to set the gain for each subband.

At the time of writing, data are not provided in the standard PSRFITS format.

In addition to the Pulsar Backend, the Open Loop Recorder (§7.4) can also be exploited for time domain radio astronomy, as it offers a fast time sampling capability. Accordingly, we consider both here, as the desired observations may motivate choosing one backend over the other. General considerations about how to conduct specific observations are the following:

- Both backends are suitable for **search** observations, in which the pulsar's DM is either not known or may be suspected to be variable (e.g., some single-pulse studies and FRB observations).
- Both backends support **incoherent dedispersion**. For the Pulsar Backend, near-real time incoherent dedispersion can be performed; for the Open Loop Recorder, dedispersion is performed after the data are transferred to another processing machine.
- Both backends support **coherent dedispersion**. For the Pulsar Backend, some limited dedispersion can be performed in near-real time; for the Open Loop Recorder, dedispersion is performed after the data are transferred to another processing machine.

At the time of writing, neither backend is suitable for **precision timing**.

Tables 7.2 and 7.3 present various recommendations and constraints on the use of the two backends.

7.4 Open Loop Recorder

This material is extracted from 810-005 (2019), Module 209 (Rev. D).

Each Complex hosts eight Open Loop Recorders, designed to process signals from the standard DSN TT&C bands. The primary intention of the Open Loop Recorders is to support Radio Science experiments associated with NASA or other space agency missions, but they can also be used for radio astronomy.

An Open Loop Recorder receives one or more copies of the digitized IF from an antenna via a Complex-wide packet switch. An Open Loop Recorder can receive up to 16 IF inputs, with each IF input possibly having a different bandwidth and bit depth. Available input IF bandwidths are ("narrowband") 200 Hz to 500 kHz and ("wideband") 1 MHz to 50 MHz. The Open Loop Recorders have been validated for operational data acquisition for bandwidths up to 512 MHz (16×32 MHz), but users have reported success using bandwidths of 1024 MHz (16×64 MHz). However, the total input data rate to an Open Loop Recorder cannot exceed the 10 Gbps packet switch capacity.

Standard radio astronomy processing would configure an Open Loop Recorder to have a common configuration across all IF inputs, typicallly with IF bandwidths of 8 MHz, 16 MHz, or 32 MHz so as to cover the full IF, but it is possible to have simultaneous "wideband" and "narrowband" recording. If an antenna is configured in a "dichroic" mode to receive two (sky) frequencies simultaneously (e.g., S- and X band or X- and Ka band), the IF inputs can be distributed across the two (sky) frequencies.

Following recording, data are transferred off the Open Loop Recorder for additional processing. For time domain radio astronomy purposes, the subsequent processing can include either incoherent or coherent dedispersion. Time resolutions as fine as 31.25 ns can be achieved across the largest subband bandwidth of 32 MHz.

At time of writing, data are not provided in the standard PSRFITS format.

7.5 VLBI Radio Astronomy (VRA) Assembly

This backend is planned for deployment into the DSN in 2021. It will provide high-bandwidth recording, with data rates up to 2 Gbps.

For radio astronomical purposes, data can be obtained in the VLBI Data Interchange Format (VDIF).

Appendix A

Proposal Preparation and Observation Planning

This appendix is designed to provide a variety of information that proposers may find useful in developing a proposal or planning observations.

Figures A.1, A.2, and A.3 show the visibilities of sources as a function of hour angle and declination. These guides should be taken as approximate. All of the Complexes have local topography that can restrict the lowest available elevation at some azimuths. DSN Telecommunications Interfaces Module 301L (2019) provides specific elevation limits, as a function of hour angle, for individual antennas as well as precise antenna locations in various coordinate systems.

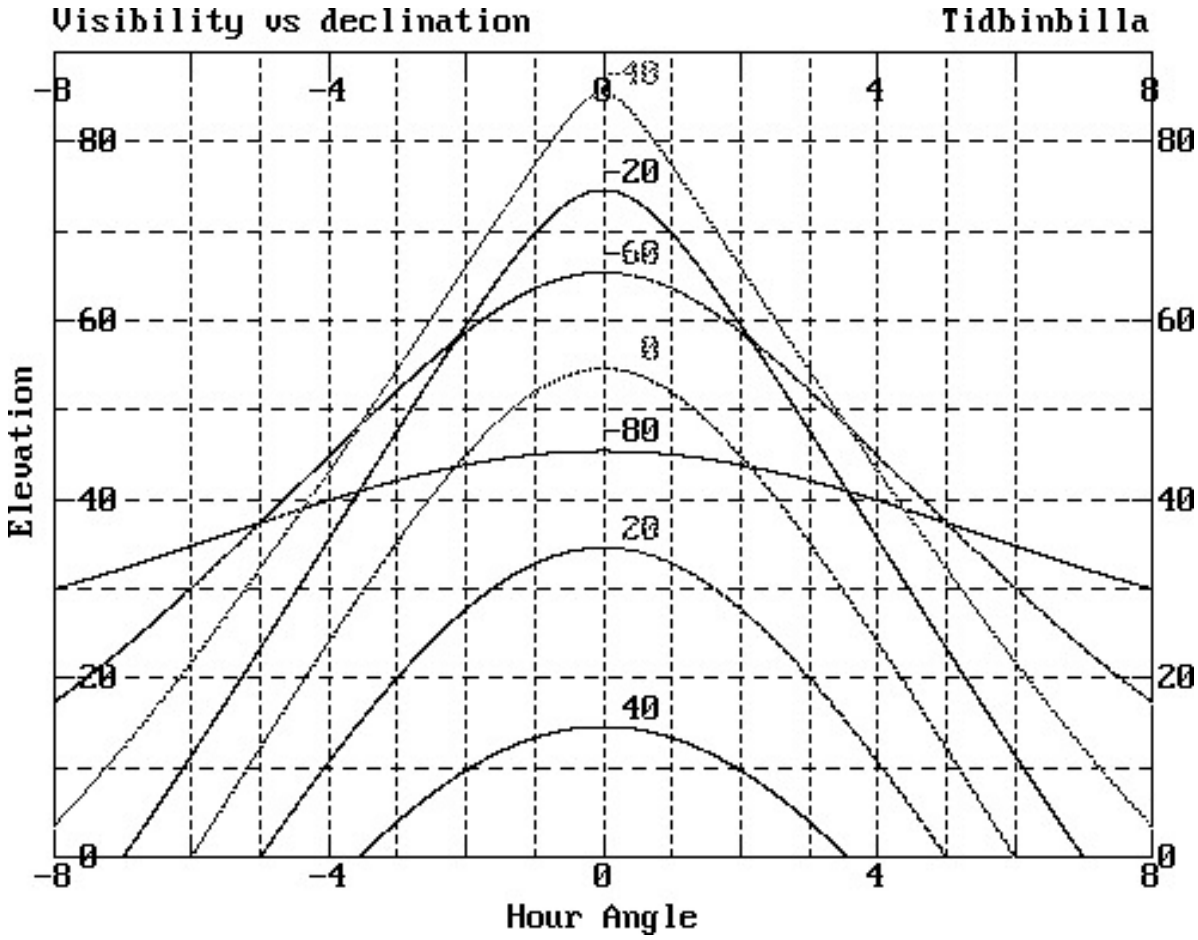

Figure A.1: Visibility of sources from the Canberra Deep Space Communications Complex. The abscissa is the hour angle, and the ordinate is the elevation. The different curves are labeled by the declination of a source.

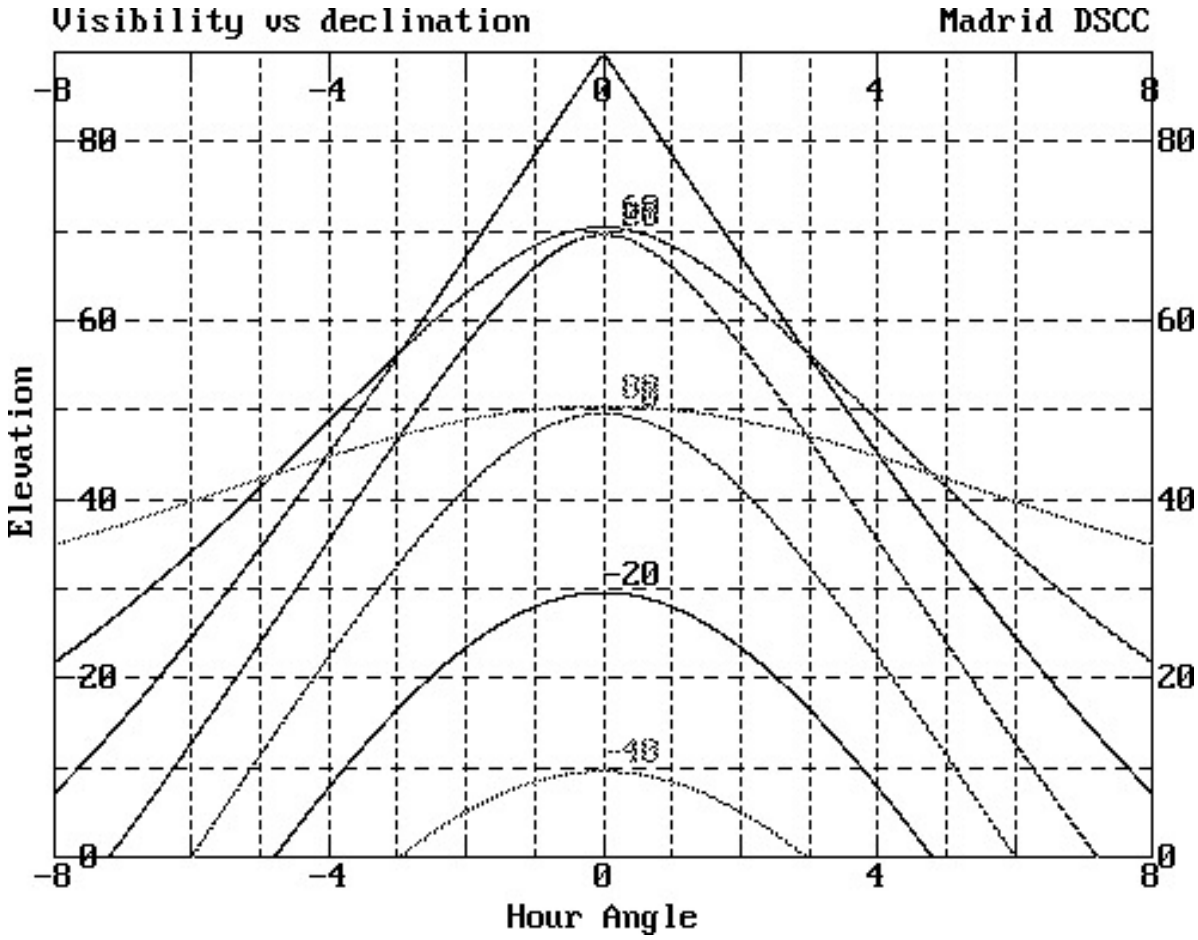

Figure A.2: Visibility of sources from the Madrid Deep Space Communications Complex. The abscissa is the hour angle, and the ordinate is the elevation. The different curves are labeled by the declination of a source.

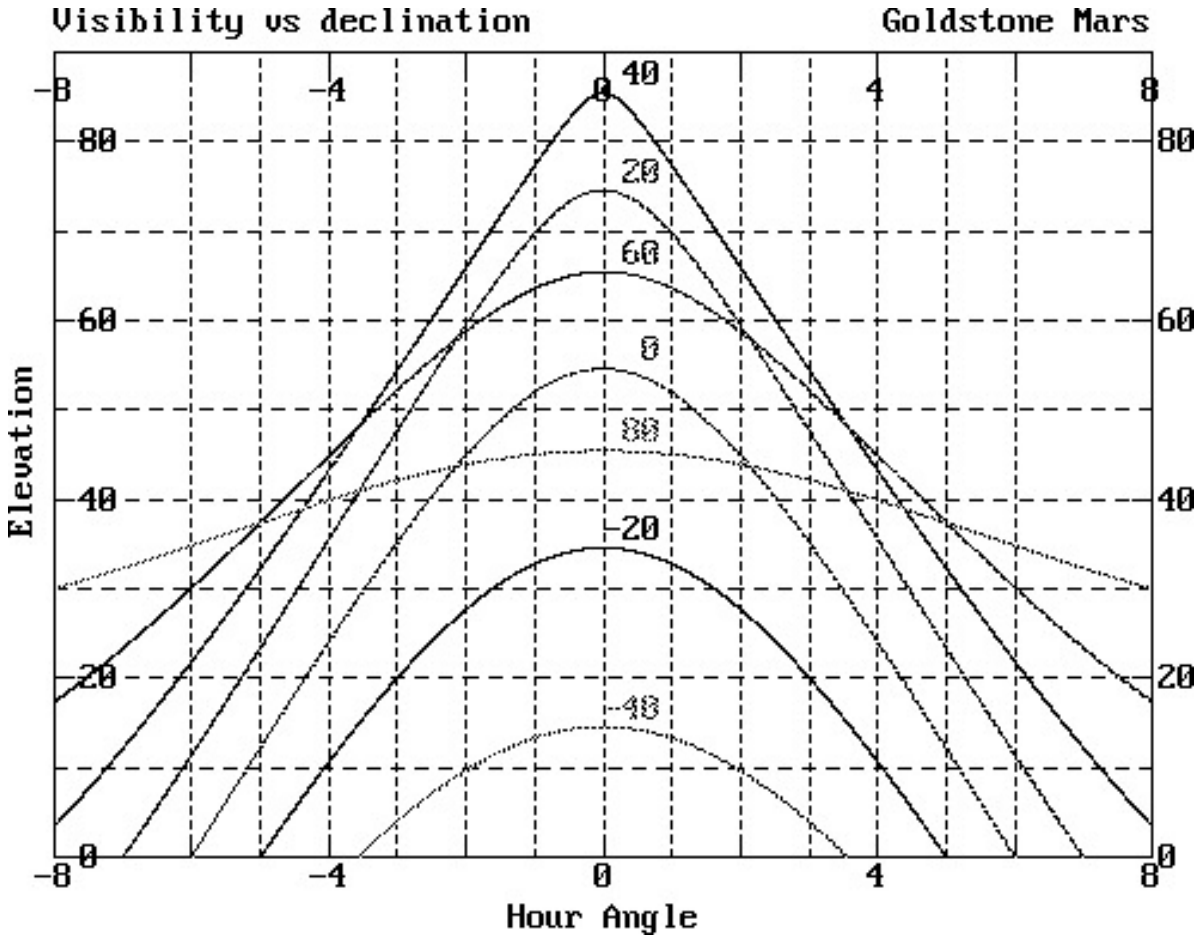

Figure A.3: Visibility of sources from the Goldstone Deep Space Communications Complex. The abscissa is the hour angle, and the ordinate is the elevation. The different curves are labeled by the declination of a source.

Bibliography

Charlot, P., et al. 2020, Astron. & Astrophys., in preparation; http://hpiers.obspm.fr/icrs-pc/newwww/icrf/icrf3-ReadMe.txt

Cohen, M. H., Cannon, W., Purcell, G. H., Shaffer, D. B., Broderick, J. J., Kellermann, K. I., & Jauncey, D. L. 1971, "The Small-Scale Structure of Radio Galaxies and Quasi-Stellar Sources at 3.8 Centimeters," Astrophys. J., 170, 207; doi: 10.1086/151204

Deep Space Network Telecommunications Interfaces, DSN No. 810-005; http://deepspace.jpl.nasa.gov/dsndocs/810-005/

Dvorsky, J., Renzetti, N., & Fulton, D. 1992, "The Goldstone Solar System Radar: A Science Instrument for Planetary Research," JPL Publication 92-29 (Jet Propulsion Laboratory, California Institute of Technology: Pasadena, CA)

Fey, A. L., Gordon, D., Jacobs, C. S., et al. 2015, "The Second Realization of the International Celestial Reference Frame by Very Long Baseline Interferometry," Astron. J., 150, 58; doi: 10.1088/0004-6256/150/2/58

Hoppe, D. J., Khayatian, B., Lopez, B., Torrez, T., Long, E., Sosnowski, J., Franco, M., & Teitelbaum, L. 2015, "Broadband Upgrade for the 1.668-GHz (L-Band) Radio Astronomy Feed System on the DSN 70-m Antennas," IPN Progress Report 42-202, Jet Propulsion Laboratory, Pasadena, CA

Garwood, R. W. 2000, "SDFITS: A Standard for Storage and Interchange of Single Dish Data," in *Astronomical Data Analysis Software and Systems IX*, Astronomical Society of the Pacific Conference Proceedings, Vol. 216, eds. N. Manset, C. Veillet, & D. Crabtree (Astronomical Society of the Pacific: San Francisco) p. 243; ISBN 1-58381-047-1

Guzman-Ramirez, L., Rizzo, J. R., Zijlstra, A. A., García-Miró, C., Morisset, C., & Gray, M. D. 2016, "First detection of $^3He^+$ in the planetary nebula IC 418," Mon. Not. R. Astron. Soc., 460, L35; doi: 10.1093/mnrasl/slw070

Imbriale, W. A. 2003, *Large Antennas of the Deep Space Network*, Volume 4, Deep Space Communications and Navigation Series, ed. J. H. Yuen, Jet Propulsion Laboratory, California Institute of Technology; (John Wiley & Sons: San Francisco, CA) ISBN: 978-0-471-44537-1

Kocz, J., Majid, W., White, L., Snedeker, L., & Franco, M. 2016, "Pulsar Timing at the Deep Space Network," J. Astron. Inst., 05, 1641013; doi: https://doi.org/10.1142/S2251171716410130

Kuiper, T. B. H., Langer, W. D., & Velusamy, T. 1996, "Evolutionary Status of the Pre-protostellar Core L1498," Astrophys. J., 468, 761; doi: 10.1086/177732

uiper, T. B. H., Franco, M., Smith, S., Baines, G., Greenhill, L. J., Horiuchi, S., Olin, T., Price, D. C., Shaff, D., Teitelbaum, L. P., Weinreb, S., White, L., & Zaw, I. 2019, "The 17–27 GHz Dual Horn Receiver on the NASA 70 m Canberra Antenna," J. Astron. Inst., 8, 1950014; doi: 10.1142/S2251171719500144

Levy, G. S., Linfield, R. P., Ulvestad, J. S., et al. 1986, "Very long baseline interferometric observations made with an orbiting radio telescope," Science, 234, 187; doi: 10.1126/science.234.4773.187

Levy, G. S., Linfield, R. P., Edwards, C. D., et al. 1989, "VLBI using a telescope in Earth orbit. I - The observations," Astrophys. J., 336, 1098; doi: 10.1086/167080

Linfield, R. P., Levy, G. S., Ulvestad, J. S., et al. 1989, "VLBI using a telescope in Earth orbit. II - Brightness temperatures exceeding the inverse Compton limit," Astrophys. J., 336, 1105; doi: 10.1086/167081

Potter, P. D. 1963, "A New Horn Antenna with Suppressed Sidelobes and Equal Beamwidths," JPL Technical Report 32-354, Jet Propulsion Laboratory, Pasadena, CA

Rizzo, J. R., Pedreira, A., García Mió, Sotuela, .I, Kuiper, T. B. H., Cernicharo, J., Castro Ceró, J. M, Larrañag,a J. R., &Ojalvo, L. 2012, "The wideband backend for host country radio astronomy in the Spanish DSN Robledo complex," in Proc. SPIE 8452, Millimeter, Submillimeter, and Far-Infrared Detectors and Instrumentation for Astronomy VI, 84522S; doi: 10.1117/12.926085

Rizzo, J. R., & García-Miró, G. 2013, "Improvements to Host Country Radio Astronomy at Robledo: Another antenna, a new receiver, a new backend," in *Highlights of Spanish Astrophysics VII, Proceedings of the X Scientific Meeting of the Spanish Astronomical Society*, eds. Guirado, J. C., Lara, L. M., Quilis, V., & Gorgas, J. p. 904

Rodriguez-Alvarez, N., Jao, J. S., Lee, C. G., Slade, M. A., Lazio, J., Oudrhiri, K., Andrews, K. S., Snedeker, L. G., Liou, R. R., & Stanchfield, K. A. 2021, "The Improved Capabilities of the Goldstone Solar System Radar Observatory," IEEE Trans. Geosci. Remote S., in press

Slade, M. A., Benner, L. A., & Silva, A. 2011, "Goldstone Solar System Radar Observatory: Earth-Based Planetary Mission Support and Unique Science Results," Proc. IEEE, 99

Velusamy, T., Kuiper, T. B. H., & Langer, W. D. 1995, "CCS Observations of the Protostellar Envelope of B335," Astrophysical Journal, 451, L75; doi: 10.1086/309691

Virkler, K., Kocz, J., Soriano, M., Horiuchi, S., Pineda, J. L., & McNichols, T. 2020, "A Broadband Digital Spectrometer for the Deep Space Network," Astrophysical Journal Supplement, 251, 1; doi: 10.3847/1538-4365/abbace